Bull. Astr. Soc. India (2002) 30, 473–490

Measurement of Solar Vector Magnetic Fields Using the Kodaikanal Tower Telescope

K. Sankarasubramanian, K.E. Rangarajan, and K.B. Ramesh
Indian Institute of Astrophysics, Bangalore-560 034, India.

Received 19 July 2001; accepted 27 February 2002

Abstract. A Stokes polarimeter was built at the Kodaikanal Tower Telescope to study the vector field map of active regions like sunspot using the well known Fe I lines 6301.5 Å and 6302.5 Å lines. The Mueller matrix of the polarimeter was obtained using simple laboratory and field tests. The instrumental polarisation due to the oblique reflections are removed before the observed Stokes profiles were analysed. The Advanced Stokes Polarimeter data analysis program (ASP code) was used to invert the corrected Stokes profiles to calculate the vector magnetic field parameters of NOAA 8951. The maximum field strength obtained at the umbra of the sunspot was 2500 Gauss. The variation of the field strength, the line-of-sight angle and the azimuthal angle along a cut which passes through the umbra resembles that of a simple round sunspot. The accuracy in the calculation of the vector field is high in the umbra and low in the outer edge of the penumbra of the observed sunspot. The range of errors in the calculation of the field strength, line-of-sight inclination angle, and the azimuthal angle of the magnetic vector are 20-100 Gauss, 1-5°, and 12-20° respectively. We also find a good fit for the observed Stokes profiles of the Ti I line at 6303.78 Å with a synthetic profile produced using the vector field parameters derived from the Fe I 6301.5 Å and 6302.5 Å lines.

Keywords : Vector magnetic fields, Stokes Polarimetry, Anomalous Zeeman Effect, Instrumental Polarisation, Sunspot

1. Introduction

All manifestations of solar activity like sunspots, plages, pores, flares, prominences, spicules, are caused by magnetic fields. The role of magnetic field is reflected not only in the large structures but also in the small structures like the bright points (Muller, 1985).

These small scale magnetic features are predicted to be associated with the heating of the upper layer of the solar atmosphere (van Ballegooijen, 1986). However, the physical processes behind the formation of these different scale structures are not yet clearly understood (Thomas, 1992).

In order to understand the various physical mechanisms which form different structures on the solar surface at different scales, it is necessary to quantitatively study the magnetic fields. Although qualitative information on the presence of magnetic fields and the shapes of the field lines can be obtained by observing the shapes of the structures with filters at various wavelengths, quantitative information requires polarisation measurement. The only consistent and quantitative way of studying the magnetic fields on the sun is through polarimetry (Stenflo, 1994). A recent article on the measurement of magnetic fields in Sun using Zeeman effect (Lites, 2000) gives useful references and a good explanation of the phenomenon. The inference on the field strength of magnetic field from the Zeeman splitting is possible only in the infra-red region. In the visible wavelength region, the thermal broadening of spectral line is usually higher than the Zeeman splitting restricting the calculation of field strength from the line splitting only in the umbral region of sunspots where the field strength is the highest.

With the success of the inversion codes, the measurement of full Stokes profiles or the Stokes polarimetry brings out much more physical insight of the active region than the vector magnetograph based systems (Socas-Navarro, Trujillo Bueno, and Ruiz Cobo, 2000; del Toro Iniesta & Ruiz Cobo, 1996; Skumanich & Lites, 1987). It is now realised that a Stokes polarimeter is essential in any solar observatory in order to understand the magnetic field structure on the sun. Since, the Kodaikanal Tower Telescope (KTT) (Bappu, 1967) has a high resolution spectrograph with spectral resolution comparable to the spectrograph used by the Advanced Stokes Polarimeter (ASP), a Stokes polarimeter at KTT was built.

There were attempts to build a Stokes polarimeter in India (Balasubramaniam, 1988; Ananth *et al.*, 1994). However, until now the measurements are limited to the line of sight magnetic field (Mathew, 1998). In this paper, we report on the development of a Stokes polarimeter using the KTT to study the magnetic field of a sunspot. After successfully handling the main difficulty of removing the telescope polarisation because of oblique reflection within a percent accuracy (Sankarasubramanian *et al.*, 2000), it is now possible to study the vector magnetic fields using such an oblique reflecting telescope. We present the vector field map of an active region using this instrument.

2. Instrument

The Stokes polarimeter designed for the KTT is used in the converging beam of the telescope since the f-ratio of the telescope is high (f-90). The polarimeter consists of a manually insertable quarter waveplate (QWP), a rotating Glan-Thompson prism polaroid

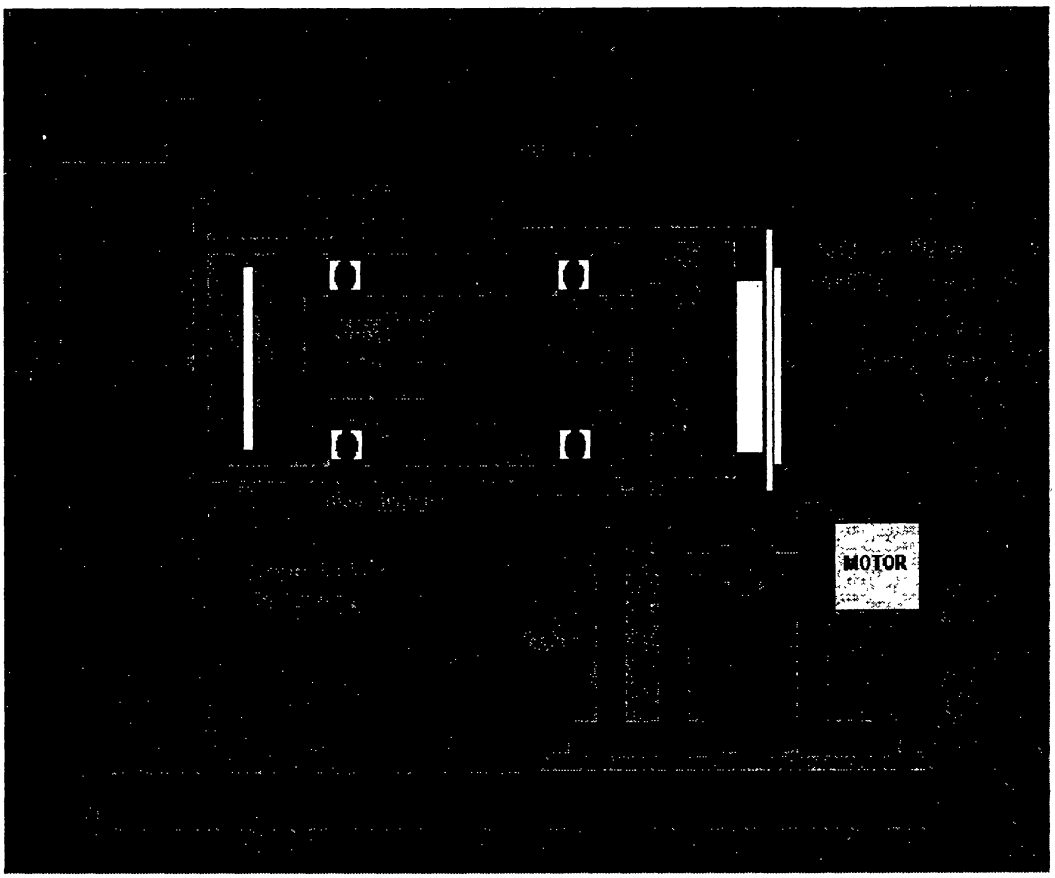

Figure 1. Schematic diagram of the Stokes polarimeter

(GTP) as analyser and an insertable polaroid (called as compensating polaroid) for the Stokes U-measurement (Figure 1).

An IR sensor with the associated electronics is used to sense the reference position which is set at 45° from the slit direction in this case. The transmission axis of the GTP is matched with the sensor position. The compensating polaroid for the Stokes U-measurement is used to compensate the spurious polarisation produced because of the differential grating response to the two orthogonal polarisation, one along the grating groove direction and the other perpendicular to it. The details of the grating response to different input polarisation state and the function of the compensating polaroid was discussed in Sankarasubramanian *et al.*, (2000). The whole polarimeter slides on to the slit of the spectrograph in order to minimise vignetting since the polarimeter is used in the converging beam of the telescope. The image plane of the telescope coincides with the slit of the spectrograph. The objective of the telescope can be moved to adjust the focal plane. Since the focal ratio of the objective is f-90, it has a very large depth of focus. Any minor defocusing due to the polarimetric optics can be readjusted by repositioning the

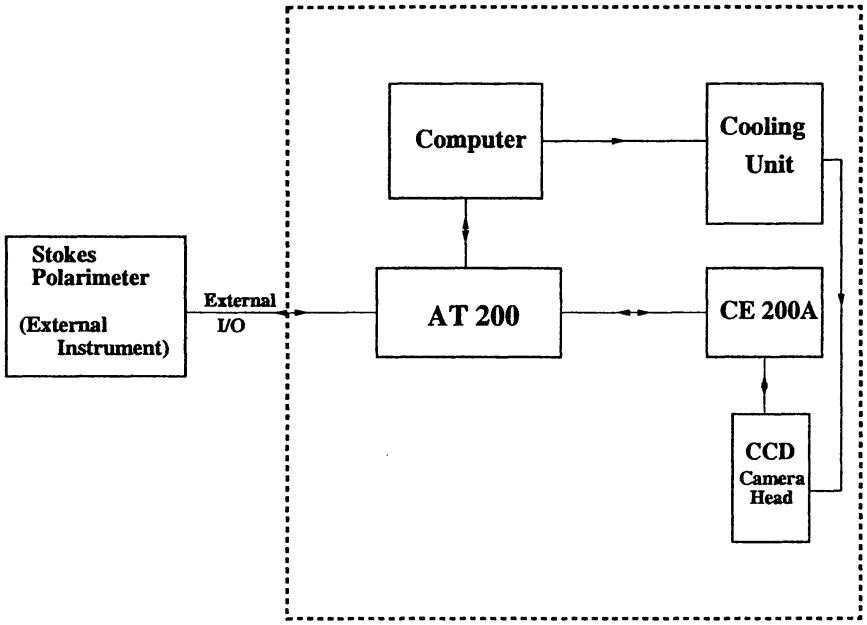

Figure 2. Block diagram of the detector and its controller units

imaging objective of the telescope. The acceptance angle constraint posed by the polariser and the QWP is well within the focal ratio of the telescope.

2.1 Spectrograph

The spectrograph is a Littrow mount type whose entrance slit is located at the image plane of the KTT. It is housed in a long cylindrical tube running along the length of the tunnel in order to reduce the scattered light. The light from the slit of the spectrograph falls on an 18.3 m focal length, two-element Hilger achromat, in conjunction with a 600 lines/mm Babcock grating, ruled over an area of 200×135 mm and blazed in the fifth order at $\lambda\lambda$5000 Å. The theoretical resolving power of the spectrograph is 600,000. The advantage of the Littrow mount spectrograph is that the Hilger achromat itself acts as a camera lens to image the spectrum on to a CCD which is kept below the slit. A one-to-one correspondence exists between every point along the length of the slit and the length of the spectrum in a direction perpendicular to the dispersion direction.

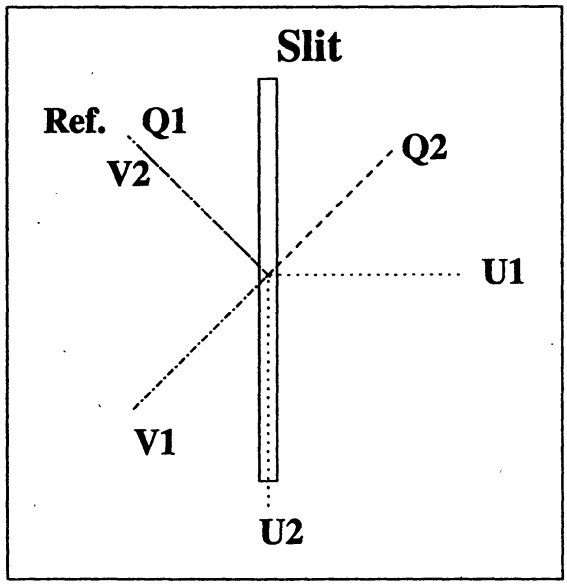

Figure 3. Schematic representation of the positions of GTP for the measurement of the four Stokes parameters. Two orthogonal position measurement will give one Stokes parameters, for example measurement at Q1 and Q2 is used to calculate Q and etc.

2.2 Detector

The detector used for this observation was a Photometrics AT200 CCD camera system. It includes three hardware components, (i) An AT200 camera controller, (ii) A CE200A camera electronics unit and (iii) A liquid cooled CH250 camera head. A liquid circulation unit is used for the cooling of the camera head. These components are linked by custom cables and controlled by a host computer. Figure 2 shows a block diagram of these units.

AT200 camera controller: The AT200 camera controller manages communications between a host computer and a CE200A camera electronics unit. A digital signal processor sends control signals to the CE200A via the camera controller cable. CCD data are received through the same cable. The AT200 has no memory of its own, so incoming data must be promptly stored in host RAM. Once collected into host memory, the data can be manipulated by software on the host computer. The AT200 can be synchronised to external equipment or to a manual trigger with the User I/O connector. This feature is used to control the Stokes polarimeter, like sensing the reference position and rotating the stepper motor.

CE200A camera electronics unit: The CE200A camera electronics unit contains signal processing, camera control, and temperature control systems. It produces CCD

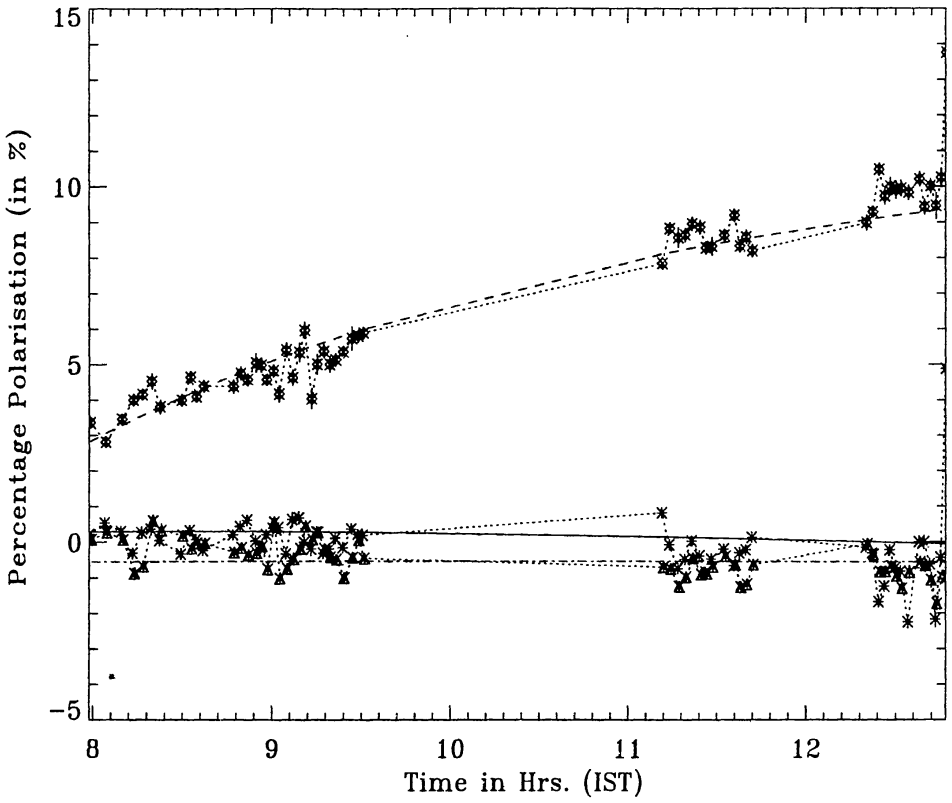

Figure 4. The time variation of the instrumental polarisation observed on the 12 April 2000 is plotted as data points. The best fitted KTT model is overplotted as solid line for Q, dashed line for U and dash-dotted line for V. To get UT, add $5^{hr}30^{min}$ to the Indian Standard Time (IST).

clocking signals for the CCD camera head and manages the transfer of raw CCD data to the AT200.

CCD camera heads: Photometrics CCD camera head is cooled to reduce dark current, the spontaneous charge generated by heat and other non-photon sources. Cooling is achieved by thermoelectric (peltier) cooling. The camera head is composed of a sealed CCD enclosure, a shutter assembly. The head contains electronics that are directly associated with CCD operation. The camera head cable transmits voltages and signals to and from the CE200A. A preamplifier raises the CCD output signal to a high level for digitisation.

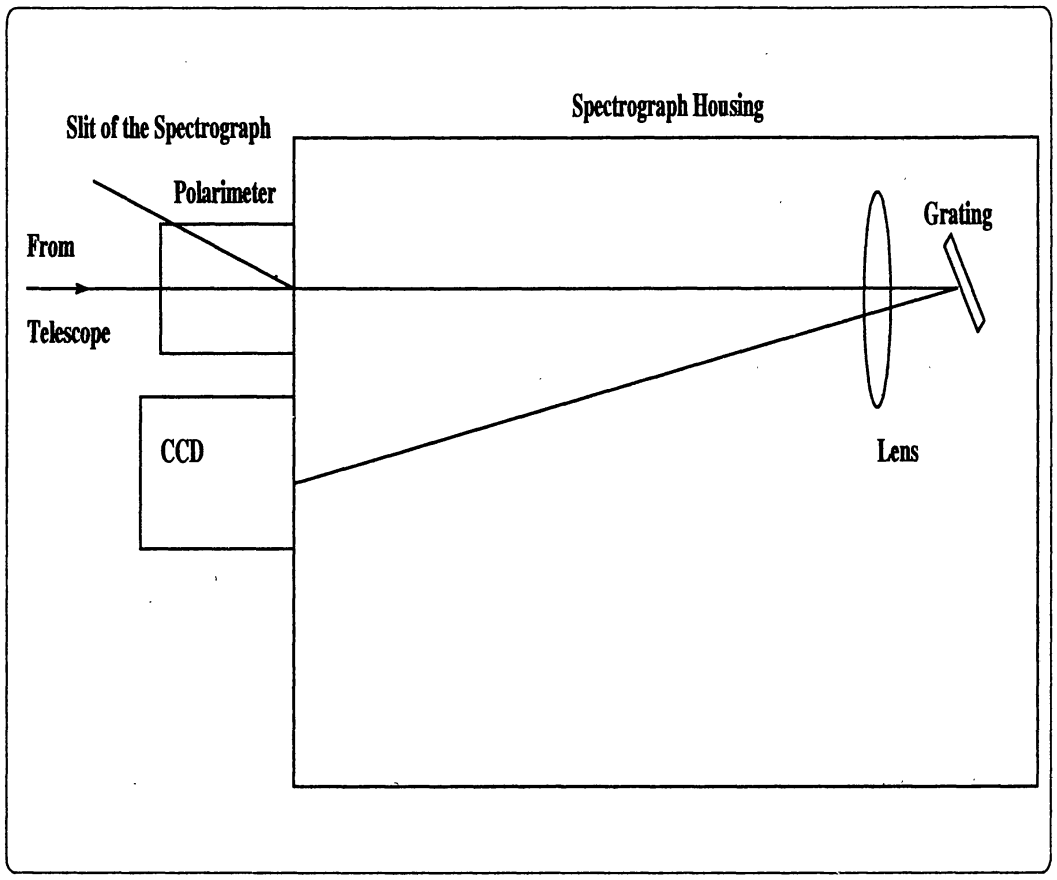

Figure 5. The schematic view of the observational setup used for the vector field measurement of the active region NOAA 8951.

2.3 Function of the Polarimeter

Figure 3 shows the schematic of the GTP positions for the measurement of different Stokes parameters. The IR-sensor position matches with the reference position marked (as Ref.) in Figure 3. This position is 45° from the slit direction. At first the polarimeter senses the reference position using the IR-sensor and the GTP is positioned for the Q1 (which is I + Q) measurement. The spectra corresponding to this position is exposed. The exposure time used for our observations varies from 100 msec to 500 msec depending on the sky transparency to achieve a good signal to noise ratio. The spectra exposed is transfered to the buffer and the polarimeter rotates to position the GTP for the orthogonal polarisation, marked in Figure 3 as Q2, and an exposure is taken to complete one Stokes' measurement. Instead of coming back to the reference position again, the polarimeter is rotated forward by 45° and then 90° more to obtain the I±U spectra (position U1 and U2 in Figure 3). This avoids the error due to backlash. The compensating polaroid is inserted behind the GTP (Figure 1) for the U measurement. This is to avoid the difference in response for the U1 and U2 measurements since those are perpendicular and parallel respectively to the

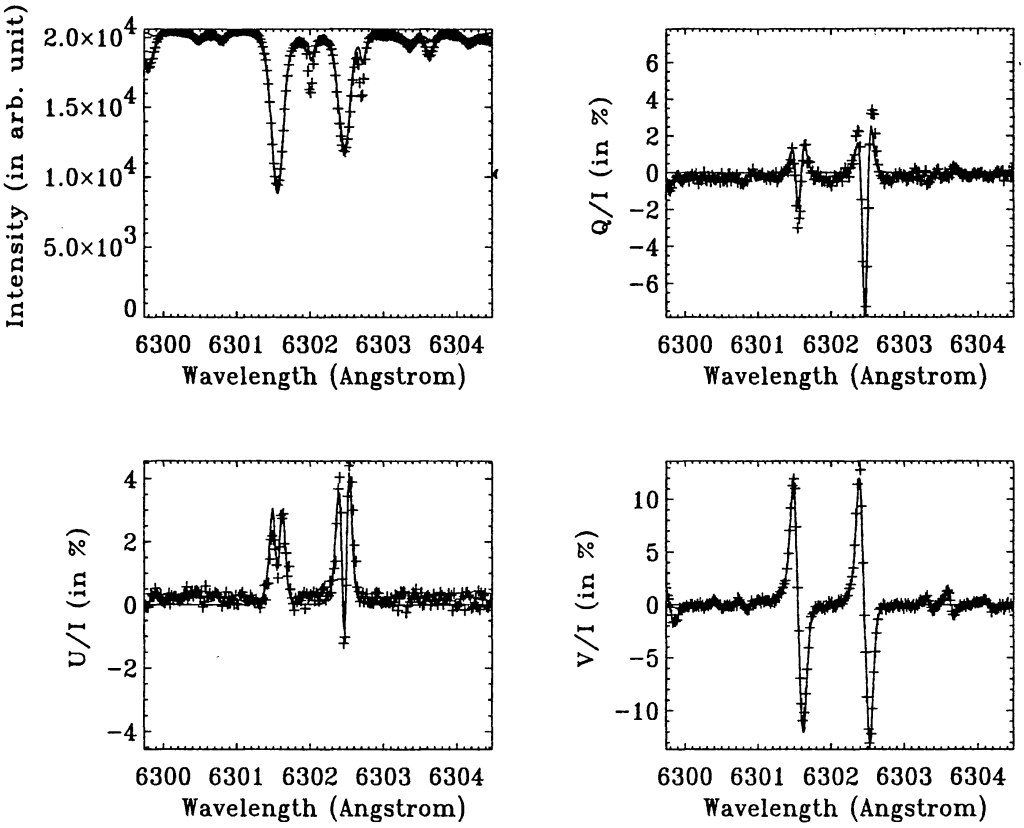

Figure 6. The observed and fitted Stokes profile at a point in the active region NOAA 8951. The point is chosen in the penumbra where all the Stokes parameters have considerable signal. The derived atmospheric parameters after the fit are, B = 1482.26±15.7 Gauss, ψ = 48.70°±0.54°, χ = -156.37°±0.83°, λ_o^m = -280.16±17.55 msec^{-1}, η_0 = 7.15±0.39, $\Delta\lambda_D$ = 28.28±0.81 m Å, a = 0.33±0.02, B_0 = 0.12±0.03, B_1 = 0.43±0.01, f = 0.36±0.03

grating groove direction. Similarly, the I±V measurement is carried out by rotating the polarimeter to 45° and then 90° more from the end position of U-measurement (marked as V1 and V2 in Figure 3). The compensating polaroid is removed and a QWP is inserted in front of the GTP for the V-measurement.

At the end of the measurement of all Stokes parameters, the GTP would have come back to the initial position (see Figure 3) and will be ready for the next measurement. All these six images were stored in the buffer. At the end of the V-measurement (V2 position of GTP), the three dimensional data cube is saved into the computer memory in 'FITS' format. The control software is written using the macros available with the Photometrics software. This includes the sensing of the initial position using the IR sensor, movement of the stepper motor to rotate the GTP and controlling the mechanical shutter in front of the CCD to expose the spectra at the correct moment. With the availability of a

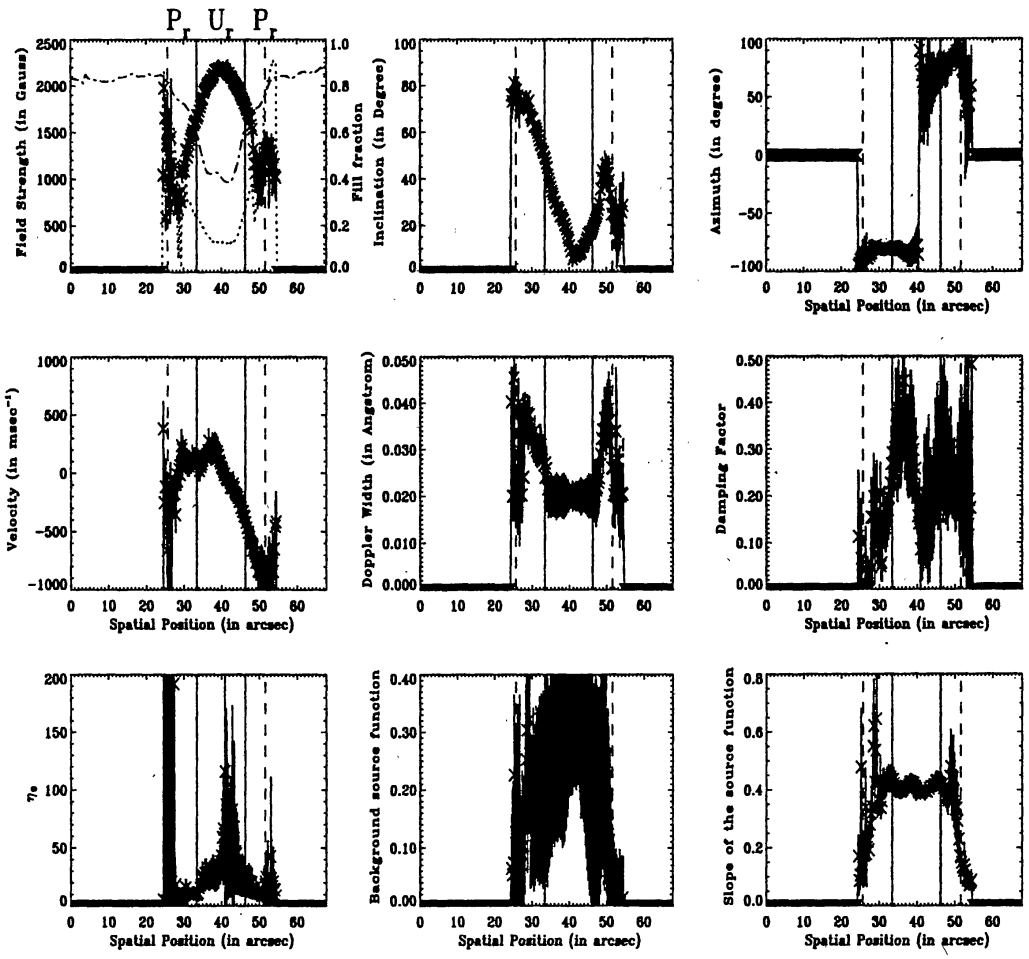

Figure 7. Plot of the physical parameters derived from the inversion. The plot has the vector field and thermodynamic parameters at a slit position which passes through the umbra of the sunspot. The left topmost plot shows the field strength variation (as solid line), the dashed line is the plot of the intensity to show the position of the umbra or the minimum intensity region. The dotted line in the same plot represents the contribution from non-magnetic region or the fill-fraction. It can be seen that the fill-fraction is less in the umbra compared to the penumbra. The symbol P_r and U_r represents the umbral and penumbral region. The solid vertical line drawn in the same plot specifies the visible umbral edge whereas the dashed line specifies the visible penumbral edge. The error bars are the errors derived from the fit and the length is five times the error derived.

pentium processor, these measurements are done quickly. All the six measurements for a slit position is done within about 1 minute. This way of measurement will introduce spurious polarisation signal if the sky condition is not good.

The polarimeter was tested in the laboratory and in the field with the KTT before the data for the sunspots were obtained (Sankarasubramanian *et al.*, 2000). The retardance

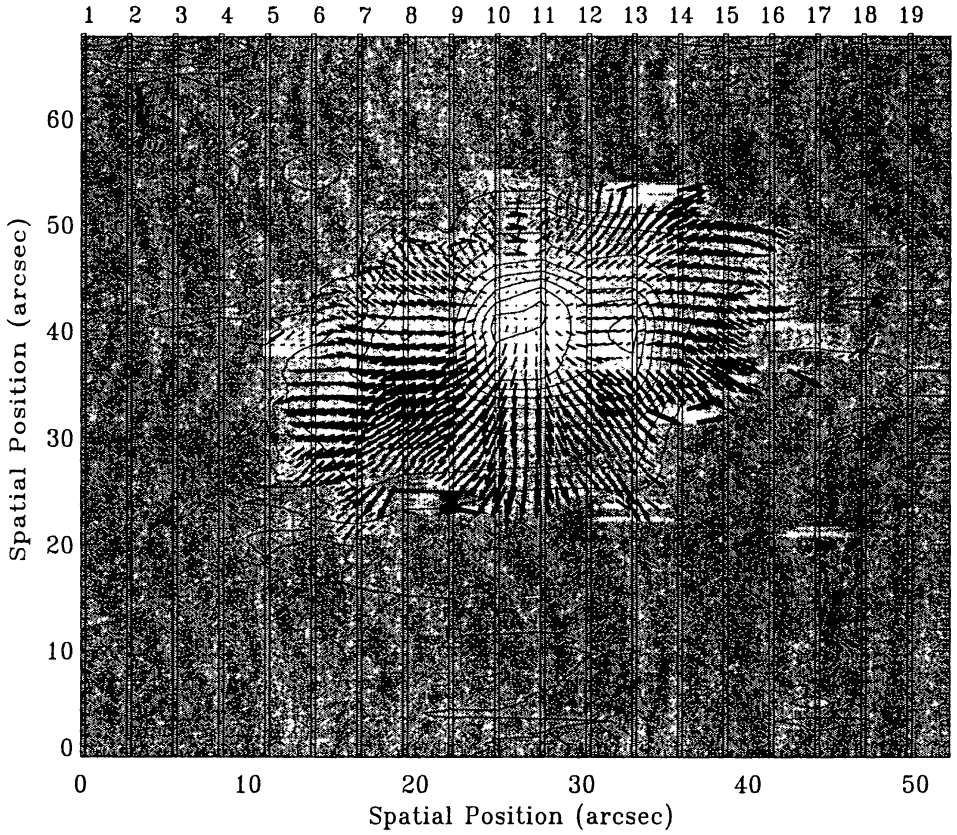

Figure 8. Vector field map of the observed active region NOAA 8951. The vertical rectangular box shown in the figure corresponds to the slit and the width corresponds to the slit width used. The grey scale represents the longitudinal field strength (brightest corresponds to a longitudinal field strength of +3000 Gauss and the darkest correspond to -3000 Gauss) and the arrows represent the transverse field strength (largest arrow corresponds to a transverse field strength of 3000 Gauss and smallest corresponds to 0 Gauss). The contour map is the intensity contour of the observed region. The data points in between the slit positions were obtained using interpolation.

error in the QWP is tested using a polarisation interferometric technique (Sankarasubramanian and Venkatakrishnan, 1998). Also, the positional alignment error of the QWP, the GTP and the compensating polaroid is tested in the laboratory (Sankarasubramanian *et al.*, 2000). All these measurements indicated an error less than 2° in the positional accuracy of the different optical components. The error in the retardance of the QWP were found to be 5.5°. An algorithm is used to find out the Mueller matrix of the polarimeter when errors are present in the alignment of the optic axis of the QWP, retardance of the QWP and the alignment of the GTP, the compensating polaroid. This algorithm is also used to remove the cross-talks between the Stokes parameters introduced by the polarimeter alone (see the Appendix-A of Sankarasubramanian (2000) for the algorithm).

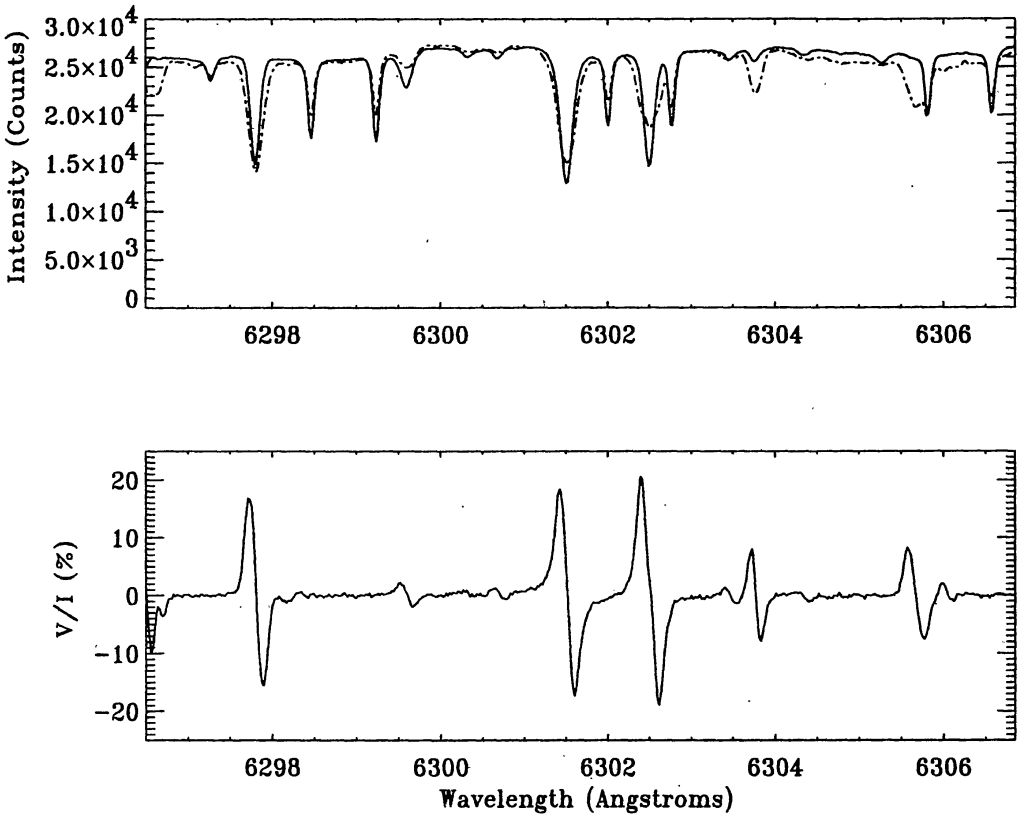

Figure 9. The spectral line profiles observed in the umbral region of the sunspot NOAA 8951. The top figure shows the intensity profile of a particular point in the umbral region of the sunspot. The solid line is the intensity spectrum obtained in the photosphere and the dash-dotted line is the intensity spectrum obtained from the umbra of the sunspot. The bottom figure shows the V-profile from the umbral region. The small self reversal in the blue wing of Ti I and in the red wing of Sc I line is due to blends.

3. Instrumental Polarisation

The Kodaikanal tower telescope is a 3-mirror coelostat system (Bappu, 1967). The oblique reflection at the three mirrors of KTT produces varying cross-talk between the Stokes parameters. The amount of cross-talk changes with time since the reflecting mirrors have to track the sun. Hence, the calibration of the telescope polarisation is essential in order to get the correct Stokes profiles from the observed one. A brief description of the scheme used to correct the telescope polarisation and the results obtained for this observing run is given in this section (see Sankarasubramanian (2000) for more details).

Sankarasubramanian *et al.*, (2000) showed that the observed time variation of the continuum polarisation matches very well with the theoretical model developed for KTT by

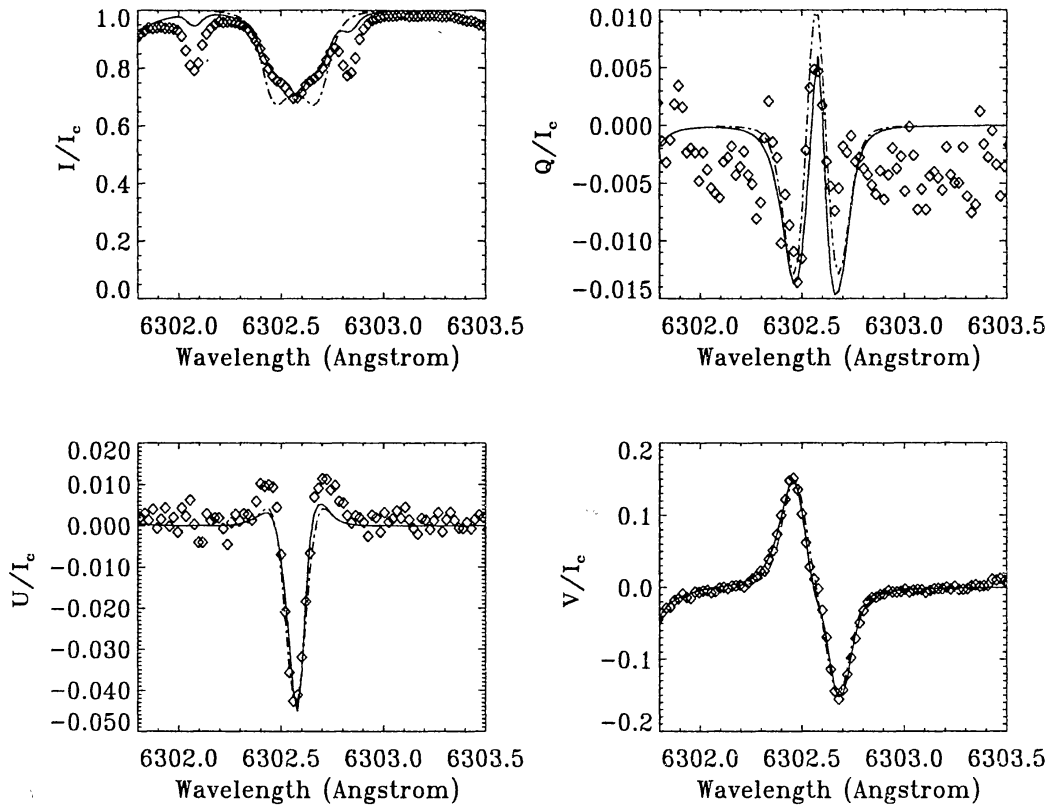

Figure 10. The observed profile of 6302.5 Å line in the umbra of sunspot NOAA 8951 is shown as diamonds. The two fitted profiles are obtained using the ASP-inversion procedure (as solid line) and the code developed for inverting the Ti I line (as dash-dotted line).

Balasubramaniam *et al.*, (1985). However, one needs to include an oxide layer parameter in the model in order to get a more accurate result (Sankarasubramanian, Samson, and Venkatakrishnan, 1999). In order to get the time variation of the continuum polarisation, we observed a non-active region in the sun center on 12 April, 2000. The continuum polarisation in the disc center is much less than the detection limit of the polarimeter (which is fraction of a percent in our case). The time variation of the Stokes parameters Q, U and V is fitted with the KTT model with the refractive index of the aluminium coating and the thickness of the oxide layer taken as free parameters. Figure 4 shows the observed Q, U and V as data points and the best fitted model data. The output of this least square fits are the refractive index of the aluminium coating and the thickness of the oxide layer of the three mirrors. We find that the data fitted better with zero oxide layer thickness. This is reasonable since the mirror was re-aluminised few months before the observation. The result of the measurements are, the real part of the refractive index, $\eta = 1.31$, the imaginary part of the refractive index, $\kappa = 7.80$. These values were input in the KTT model, for the actual observation, to get the Mueller matrix of the KTT. The

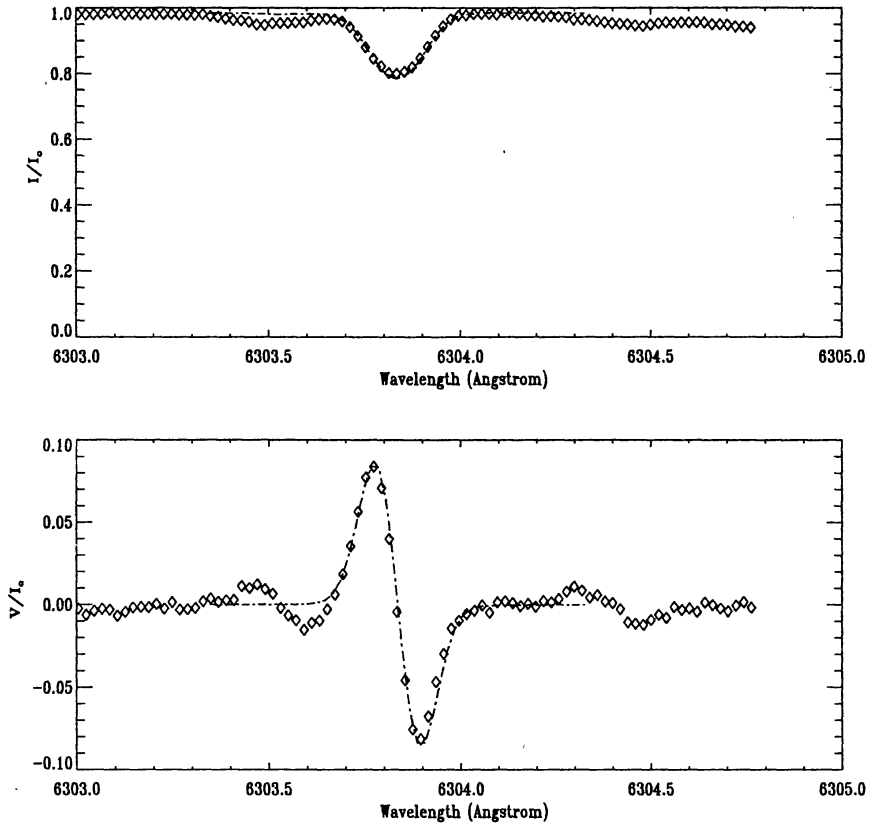

Figure 11. The observed Ti I line profile at λλ 6303.78 Å in the umbra of the sunspot NOAA 8951 is shown as diamonds. The fitted profile using the anomalous Zeeman property and with the vector field parameters derived from the Fe I lines at λλ 6301.5 Å and at λλ 6302.5 Å is shown as dash-dotted line. The Q & U profiles are within the noise level of the polarimeter.

inverse of the Mueller matrix is multiplied with the observed Stokes profiles in order to get un-corrupted Stokes profiles. The residual telescope cross-talk left after this inversion was found to be less than 0.5%.

4. Observations and Analysis

The sunspot KKL 21551 (NOAA 8951) was observed on 13 April 2000 using the polarimeter and the CCD detector described above. The observational parameters are listed in Table I and the observational configuration is shown in Figure 5. The instrumental polarisation is removed from the observed Stokes profiles using the continuum polarisation observation as explained in the last section. The corrected Stokes profiles are then inverted, using the inversion procedure developed by Skumanich and Lites (1987), for the physical parameters in the observed region. This code uses a non-linear least square

fit of the observed Stokes profiles with the synthetic profiles obtained from the Unno-Rachkovsky solutions of the polarised radiative transfer equations. This inversion code assumes the Milne - Eddington (ME) atmosphere and returns the following parameters, (i) The magnetic field strength, B, (ii) Magnetic field inclination from the line of sight (LOS), ψ, (iii) Azimuthal angle of the magnetic field vector, χ, (iv) LOS velocity represented as the line core position, λ_o^m, (v) Ratio of continuum to line absorption coefficient, η_0, (vi) Doppler width, $\Delta\lambda_D$, (vii) Damping factor, a, (viii) Constant background source function, B_0, (ix) The slope of the source function, B_1. The tenth parameter, scattered light 'f' is taken as another free parameter if the inversion includes the total intensity. This code also derives the errors in each of the fitted parameters.

Table 1. Observational parameters of the spectrograph, the Stokes polarimeter and the active region NOAA 8951.

Spectral Range covered:	6296.50 to 6306.85 Å.
Spectral Resolution :	138 210 at 6302 Å.
Dispersion:	20.25m Å per pixel.
Spatial Scale:	0.121 arcsec per pixel.
Slit Width:	0.55 arcsec.
Step Width:	2.75 arcsec.
Integration Time:	200 to 500 msec.
First Mirror Position:	East.
Date of Observation:	13 April 2000.
Time in UT Hours:	02:30 Hrs.
Field of View :	52.25×68.0 arcsec^2
Active region :	NOAA 8951.
Position on the sun:	N17°E8°.

Figure 6 shows the observed and fitted Stokes profiles at a point on the observed active region. The point is chosen in the penumbral region so that all the Stokes parameters will have a good signal to noise ratio. The caption of Figure 6 also lists the derived atmospheric parameters of the fitted penumbral point. Figure 7 shows the derived physical parameters like the total field strength, LOS inclination, the azimuthal angle of the magnetic field vector etc., for a slit position which passes through the umbral portion of the active region NOAA 8951. The error bars marked in these figures are the errors derived from the fit for the respective quantity. The length of the error bar is equal to five times the error value derived by the inversion code. The dash-dotted line in the left topmost plot of the Figure 7 is the arbitrarily scaled intensity plot to show the minimum intensity region or the umbral position. The fill-fraction which refers to the non-magnetic contribution, is plotted as a dotted line in the same plot. It can be seen that the umbra has a very little non-magnetic contribution, whereas the penumbra has a large contribution from the non-magnetic region surrounding the sunspot. Figure 7 also includes vertical lines to represent the umbral and penumbra portion. The two solid vertical lines are the edge of

the visible umbral region and the two dashed lines are the edge of the visible penumbral region. The error bar in the azimuthal angle plot shows larger value beyond the 40 arcsec position. This is due to the line-of-sight effect. In our observation, the data points beyond 40 arcsec has an angle with the line-of-sight smaller compared to the data points within 40 arcsec position. Hence, the V-signal (circular polarisation, produced by the line-of-sight magnetic field) will be quite high compared to the linear polarisation signal (Q and U profiles produced by the transverse field). Since the azimuth is calculated using the Q and U signal, the errors in the inversion is larger. Figure 7 also shows the doppler velocity derived from the inversion. The doppler velocity plot shows a flow towards the observer (negative velocity or blue shift) above the 40 arcsec position. The point below 40 arcsec shows a small flow away from the observer (positive velocity or red shift). This flow is the well-known Evershed effect first observed at the Kodaikanal telescope, (Evershed, 1909) and recently Title et al. (1992) showed that the flow is confined to the penumbral dark filaments.

The step width for the slit position used for these observations is 2.75 arcsec. Even though the step width is not sufficient for a high resolution vector field map, a map was produced using these observations and shown in Figure 8. The vector fields for the regions between the slit positions are derived by interpolation using the 'congrid' routine in IDL (Interactive Data Language). The 180° ambiguity in the azimuth was corrected manually by looking at the sudden jumps in the azimuthal map. However, there are several methods to resolve this ambiguity (see for e.g., Metcalf, 1994) and can be implemented into the software. The gray scale image shows the longitudinal field strength. Higher intensity values represent higher longitudinal field strength. The transverse field strength is depicted as the magnitude of the arrow and the direction of the arrow is determined from the azimuthal angle of the field. The rectangular box marked in the Figure 8 is the slit positions used for the observation and the width corresponds to the slit width used. The intensity map of the region is depicted as contours. The increasing numbers marked are the direction in which the slit was stepped to complete the map of the active region. The errors in the inferred vector field parameters are the following, (a) In the umbra, the errors in the field strength, LOS-inclination angle and the azimuthal angles are 20 Gauss, 1° and 5° respectively, (b) In the outer edge of the sunspot it is, 100 Gauss, 3° and 12° respectively and (c) In the small-scale fields surrounding the sunspot, it is 120 Gauss, 5° and 20° respectively.

5. Discussions & Conclusions

In this paper, we described the development of a Stokes polarimeter for the Kodaikanal tower telescope. The instrumental polarisation is corrected off-line using the continuum polarisation measurement taken a day before the actual observation in conjunction with the KTT model. The residual cross-talk left after the off-line correction was found to be less than 0.5%. The sunspot NOAA 8951 was observed in order to obtain its vector magnetic field. After correcting for the instrumental polarisation, the Stokes profiles are

inverted using an inversion procedure used for the Advanced Stokes polarimeter data. The vector field map was produced using the results obtained from this inversion.

The removal of the instrumental polarisation from the observed Stokes profiles makes the vector field calculations more accurate and consistent. Also, the use of large format CCD (1K×1K) gives a large field of view measurement and more spectral lines apart from the Fe I lines at $\lambda\lambda$ 6301.5 Å and at $\lambda\lambda$ 6302.5 Å lines. For example see the subsection on the anomalous Zeeman effect. Even though the system as of now can be used for studies of sunspot magnetic field with field strength greater than few hundred Gauss, we list some of the improvements which will definitely boost the performance of the whole system.

(i) The mapping of an active region was obtained by moving the image on the slit of the spectrograph. This was done manually and hence the step size was about 2.75 arcsec. The mapping with this coarse step size does not give us a high-spatial resolution vector field map and hence the finer structures in the penumbral regions. An automatic guiding system is essential for a high-spatial resolution vector maps.

(ii) Even though the high-spatial resolution mapping of an active region could be possible with an automatic guider and finer step size, it is always advantageous to have a slit-jaw picture. This will enable us to look for any systematic effects because of image motion between the two orthogonal polarisation measurements. The test carried out by us showed image motion between the orthogonal polarisation is less than one pixel. The slit-jaw picture can also be used to study the horizontal flows in and around the active regions.

(iii) With the above improvements one can obtain several scans of an active region and the time variations of the physical parameters can be studied (Lites *et al.*, 1998). At present a study of high resolution temporal evolution of sunspots is not possible in KTT because of the manual movements of the image for a single scan.

5.1 Anomalous Zeeman Effect

With the large field of view and more spectral lines within the CCD window, the spectral lines Ti I and Sc I with rest wavelength at $\lambda\lambda$ 6303.769 Å and at $\lambda\lambda$ 6305.74 Å was observed along with the Fe I lines at $\lambda\lambda$ 6301.5 Å and at $\lambda\lambda$ 6302.5 Å. The effective lande factor for these two lines are 0.92 and 1.20 respectively. Figure 9 shows the observed I and V/I profiles at a point in the observed region. The top plot of the Figure 9 shows the intensity spectrum from a non-active region (solid line) and from the umbral region of the sunspot (dash-dotted line). It can be seen from this figure that the Ti I and Sc I has more line depths in the umbral region than in the photosphere. These are low excitation lines and forms only in the cooler region on the sun and hence more prominently seen in the umbral spectrum than in the photospheric spectrum. This property will have the advantage that the field strengths and other parameters derived from these lines will have

minimum influence from the photospheric light. Also, the formation height of the Ti I line is about 70 km above the formation height of the Fe I lines (Lites *et al*, 1998), hence the calculation of vector field from Ti I and Fe I lines will give us the height variation of the vector field parameters. However, in order to invert Ti I and Sc I lines, the inversion code has to include the anomalous Zeeman effect.

A code including the anomalous Zeeman effect was developed. This code synthesis the Stokes profiles of Ti I line observed at $\lambda\lambda$ 6303.77 Å for a ME-atmosphere when the vector field parameters are given as input. In order to test the code the Stokes profiles for 6302.5 Å line were synthesised with the vector field parameters derived from the ASP-inversion procedure. Figure 10 shows the observed Stokes profiles of the Fe I line at $\lambda\lambda$ 6302.5 Å line along with the Stokes profiles derived with the ASP-inversion code (as solid line) and from this new code (as dash-dotted line).These two Stokes profiles matches quite well with each other and with the observed Stokes profiles. The I-profile shows more deviation compared to the other profiles since the code does not include the fill-fraction or the scattered light. The Stokes-U profile is very close to the noise limit and hence a small deviation from the fit. In a similar way, the synthetic profiles for the Ti I line was produced using the vector field parameters derived from the ASP-inversion of the Fe I lines. The percentage of polarisation of V is about a factor less than that of the Fe I lines at $\lambda\lambda$ 6301.5 Å and at $\lambda\lambda$ 6302.5 Å. Since, Q & U are less by a factor compared to V, the percentage polarisation of Q & U is below the detection limit of the polarimeter (below 0.5%). However, the percentage polarisation of V in the umbral region is more than 1% and hence reliable for fitting. The ratio of continuum to line absorption coefficient (η_0), the damping factor (a), and the source function (B_0 & B_1) are varied manually in order to get a good fit. Figure 11 shows the observed Stokes profiles of the Ti I line and the fitted profiles for a position in the umbral region, using the code developed. The derived values for η_0, a, and B_0/B_1 are smaller compared to the values derived for the Fe I lines confirming that the Ti I line forms at a different layer compared to the Fe I lines (Lites *et al.*, 1998).

Acknowledgments

A part of this work was done during the Ph.D. thesis of K. Sankarasubramanian whose supervisor, Prof. P. Venkatakrishnan gave excellent support and constant encouragement. We thank the observers Mr. Devendran and Mr. Hariharan for assisting us during the observing period. We thank Dr. Micheal Sigwarth and Dr. Thomas Rimmele for introducing Sankar to the ASP-inversion procedure and the inversion code. We also thank Mr. A. V. Ananth for his help in developing the required computer software, and Prof. Jagdev Singh for modernising the KTT facility and allowing us to use it.

References

Ananth, A. V., Venkatakrishnan, P., Narayanan, R. S., and Bhattacharyya, J. C., 1994, Solar

Phys., 151, 231.
Balasubramaniam, K. S., Venkatakrishnan, P., and Bhattacharyya, J. C., 1985, Solar Phys., 99, 333.
Balasubramaniam, K. S., 1988, Stokes Polarimetry and the Measurement of Vector Magnetic Fields in Solar Active Regions, Ph.D. Thesis, Dept. of Physics, Indian Institute of Science, Bangalore, India.
Bappu, M. K. V., 1967, Solar Phys., 1, 151.
Bhattacharyya, J. C., 1965, Studies of Solar Magnetic and velocity Fields, Ph.D Thesis, Dept. of Science, University of Calcutta, Calcutta, India.
del Toro Iniesta, J. C., and Ruiz Cobo, B., 1996, Solar Phys., 164, 169.
Evershed, J., 1909, Mon. Not. Roy. Astr. Soc., 69, 454.
Lites, B. W., Thomas, J. H., Bogdan, T. J., and Cally, P. S., 1998, Astron. Astrophys., 497, 464.
Lites, B. W., 2000, Rev. of Geophys., 38, 1.
Mathew, S. K., 1998, A Study of Solar Magnetic and Velocity Fields, Ph.D Thesis, Dept. of Physics, Gujarat Univ., Gujarat, India.
Metcalf, T. R., 1994, Solar Phys., 155, 235.
Muller, R., 1985, Solar Phys., 100, 237.
Sankarasubramanian, K. and Venkatakrishnan, P., 1998, Optics and Laser Tech., 30, 15.
Sankarasubramanian, K., Samson, J. P. A., and Venkatakrishnan, P., 1999, in K. N. Nagendra, and J. O. Stenflo. (eds.), Proceedings of an International Workshop on Solar Polarization, Kluwer Academic Publishers, Boston, p. 313.
Sankarasubramanian, K., Srinivasulu, G., Ananth, A. V., and Venkatakrishnan, P., 2000, J. Astrophys. Astron., 21, 241.
Sankarasubramanian, K., 2000, Solar Polarimetry: Techniques and Applications, Ph.D Thesis, Dept. of Physics, Bangalore Univ., Bangalore, India.
Skumanich, A., and Lites, B. W., 1987, Astrophys. J, 322, 473.
Socas-Navarro, H., Trujillo Bueno, J., and Ruiz Cobo, B., 2000, Astrophys. J, 530, 977.
Stenflo, J. O., 1994, Solar Magnetic Fields: Polarized Radiation Diagnostics, Kluwer Academic Publishers, Dordrecht.
Thomas, J. H., 1992, in J. H. Thomas, and N. O. Weiss (eds.), Sunspots: Theory and Observations, Kluwer Academic Publishers, Dordrecht, p. 3.
Title, A. M., Frank, Z. A., Shine, R. A., Tarbell, T. D., Topka, K. P., Scharmer, G. B., and Schmidt, W., 1992, in J. H. Thomas, and N. O. Weiss (eds.), Sunspots: Theory and Observations, Kluwer Academic Publishers, Dordrecht, p. 195.
van Ballegooijen, A. A., 1986, Astrophys. J., 311, 1001.